CMS Physics Analysis Summary

Contact: cms-pag-conveners-smp@cern.ch 2016/11/23

Measurement of Triple-Differential Dijet Cross Sections at $\sqrt{s} = 8\,\text{TeV}$ with the CMS Detector and Constraints on Parton Distribution Functions

The CMS Collaboration

Abstract

A measurement of triple-differential dijet cross sections at a centre-of-mass energy of $\sqrt{s} = 8\,\text{TeV}$ is presented using $19.7\,\text{fb}^{-1}$ of data collected with the CMS detector in proton-proton collisions at the LHC. The cross sections are measured as a function of the average transverse momentum, half the rapidity separation, and the boost of the two leading jets. The cross sections are unfolded for detector effects and compared to calculations in perturbative quantum chromodynamics at next-to-leading order accuracy complemented with electroweak and nonperturbative corrections. Constraints on the parton distribution functions are derived and the strong coupling constant is determined to be $\alpha_s(M_Z) = 0.1199 \pm 0.0015\,(\text{exp})\,^{+0.0031}_{-0.0020}\,(\text{theo})$.

1 Introduction

The pairwise production of hadronic jets is one of the fundamental processes at hadron colliders. Dijet events with high transverse momenta can be described by parton-parton scattering in the context of quantum chromodynamics (QCD). Measurements of dijet cross sections can be used to thoroughly test predictions of perturbative QCD (pQCD) at high energies and to constrain the parton distribution functions (PDFs). Earlier measurements of dijet cross sections in proton-(anti)proton collisions have been performed as a function of dijet mass at the SPPS, ISR, and Tevatron colliders [1–6]. At the LHC, dijet measurements as a function of dijet mass have been reported in Refs. [7–11]. Alternatively, dijet events have also been studied triple-differentially in transverse energy, and the pseudorapidities η_1 and η_2 of the two leading jets [12, 13].

In this paper, a measurement of triple-differential dijet cross sections is presented. The cross sections are measured as a function of the average transverse momentum $p_{\mathrm{T,avg}} = \frac{1}{2}(p_{\mathrm{T},1} + p_{\mathrm{T},2})$ of the two leading jets, half their rapidity separation $y^* = \frac{1}{2}|y_1 - y_2|$, and the boost of the dijet system, $y_{\mathrm{b}} = \frac{1}{2}|y_1 + y_2|$. The corresponding dijet event topologies are illustrated in Fig. 1.

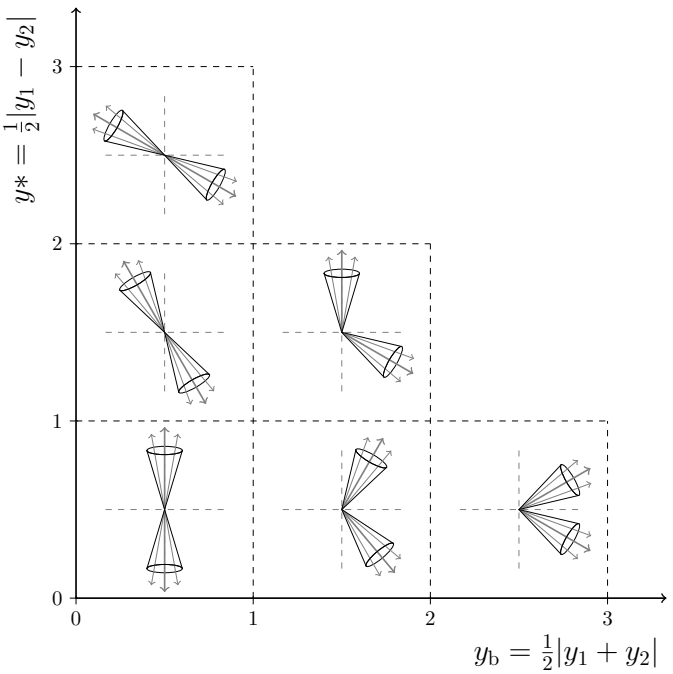

Figure 1: Illustration of the dijet event topologies in the y^* and y_{b} kinematic plane. The dijet system can be classified as a same-side or opposite-side jet event according to the boost y_{b} of the two leading jets providing insight into the parton kinematics.

The relation of the dijet rapidities and the parton momentum fractions $x_{1,2}$ at leading order (LO) is given by $x_{1,2} = \frac{p_{\mathrm{T}}}{\sqrt{s}}(e^{\pm y_1} + e^{\pm y_2})$. For large values of y_{b}, the momentum fractions carried by the incoming partons must correspond to one large and one small value, while for small y_{b} the momentum fractions must be approximately equal. In addition, for high transverse momenta of the dijets, x values beyond 0.1 are probed, where the proton PDFs are not well known yet.

The decomposition of the dijet cross sections into the contributing partonic subprocesses is shown at next-to-leading-order (NLO) accuracy from NLOJET++ [14, 15] in Fig. 2. At small y_{b} and in particular large $p_{\mathrm{T,avg}}$ a significant portion of the cross section corresponds to quark-

quark (and small amounts of antiquark-antiquark) scattering with varying shares of equal- (4) or unequal-type (5) quarks. On the contrary, for large y_b the cross section is composed by more than 80% of partonic subprocesses with at least one gluon participating in the collision. Thus, important information about the PDFs can be derived from such a measurement.

The analyzed data were collected with the CMS detector in the 2012 LHC run period at $\sqrt{s} = 8\,\text{TeV}$ and correspond to an integrated luminosity of $19.7\,\text{fb}^{-1}$. The measured cross sections are corrected for detector effects and are compared to NLO calculations in pQCD, complemented with electroweak (EW) and nonperturbative (NP) corrections. Furthermore, contraints on the PDFs are studied and the strong coupling constant is determined.

2 Event selection

The dijet events are collected using five single-jet high-level triggers [16], which require at least one jet with p_T larger than 80, 140, 200, 260, and 320 GeV, respectively. All but the highest-threshold trigger were prescaled in the 2012 LHC run. The triggers are employed in mutually exclusive regions of the $p_{T,avg}$ spectrum, see Table 1, in which their efficiency exceeds 99%.

Table 1: List of single-jet trigger paths used in the analysis.

Trigger path	$p_{T,avg}$ range (GeV)
HLT_PFJET80	123–192
HLT_PFJET140	192–263
HLT_PFJET200	263–353
HLT_PFJET260	353–412
HLT_PFJET320	412–

Particle candidates are reconstructed using the particle flow (PF) algorithm [17, 18], in which the information of all sub-detectors is combined. The leading primary vertex is chosen based on the sum of squares of all associated track transverse momenta. The subleading vertices are classified as pileup vertices, which result from additional proton-proton collisions. To reduce this bias, charged hadrons that unambiguously originate from a pileup vertex are removed within the coverage of the tracker $|\eta| < 2.4$ [19]. The jets are built from the four-vectors of the reconstructed particle candidates using the anti-k_t algorithm [20] with a jet size parameter of $R = 0.7$ as implemented in the FASTJET package [21].

The reconstructed jets need to be corrected for residual nonlinearities and nonuniformities in the detector response. The jet energy corrections (JEC) [22] are derived using simulated events and in situ measurements with dijet, photon+jet, and Z+jet events. An additional offset correction is applied to take into account the extra energy clustered into jets from additional proton-proton interactions within the same or neighbouring bunch crossings (in-time and out-of-time pileup) [22]. A small bias in the reconstructed pseudorapidity observed at the edge of the tracker is accounted for by an additional correction.

All events are required to have at least one primary vertex (PV). The PV needs to be reconstructed from at least 5 tracks and the longitudinal and transverse distances of the PV to the nominal interaction point of CMS need to satisfy $|z_{PV}| < 24\,\text{cm}$ and $|\rho_{PV}| < 2\,\text{cm}$. Nonphysical jets are removed by loose jet identification criteria with an efficiency greater than 99%.

Only events with at least two jets up to an absolute rapidity of $|y| = 5.0$ are selected and the two jets leading in p_T are required to have transverse momenta greater than 50 GeV and $|y| < 3.0$. The missing transverse momentum is the negative vector sum of the transverse momenta of

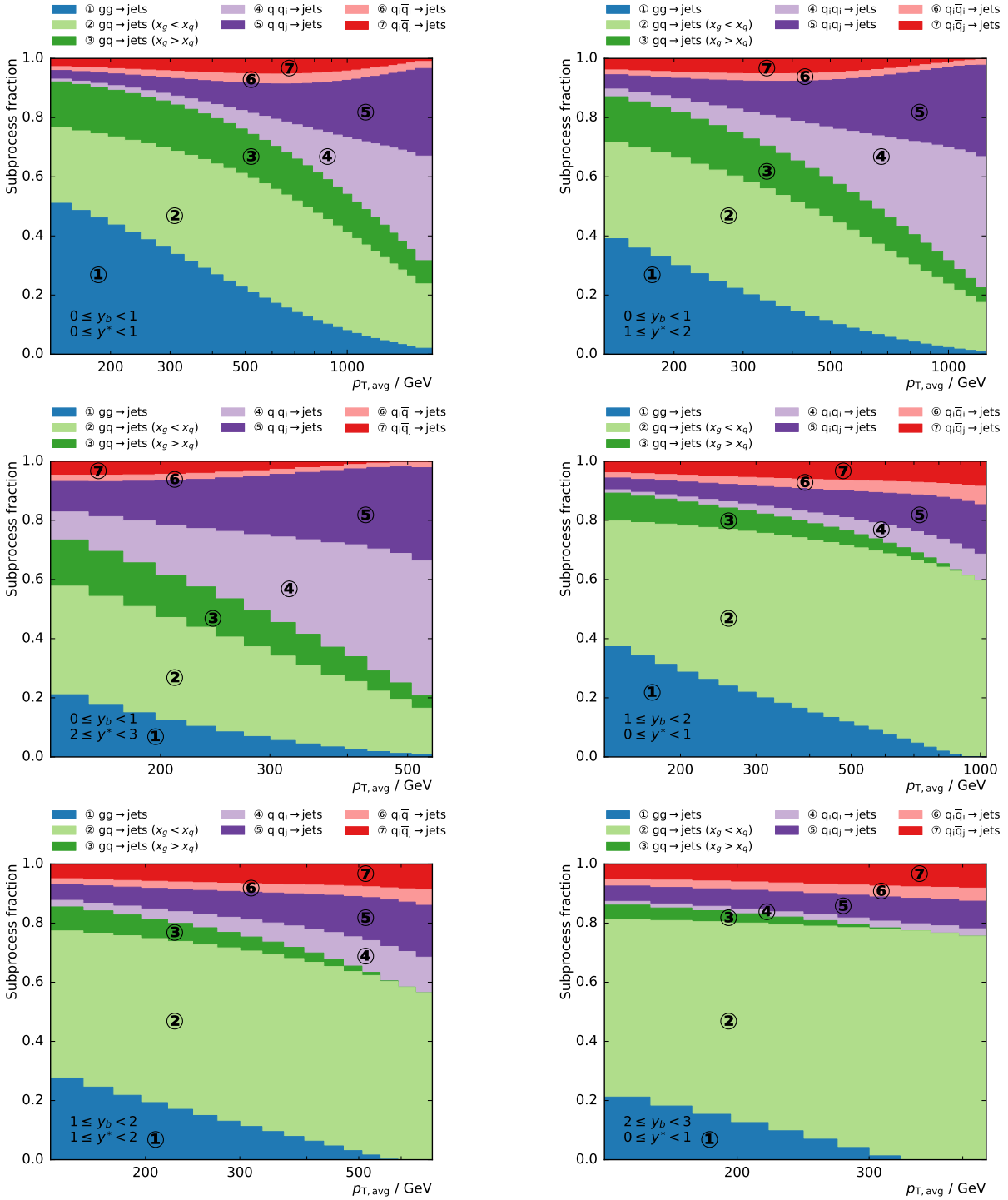

Figure 2: Relative contributions of all subprocesses to the total cross section at NLO as a function of $p_{T,avg}$ in the various y^* and y_b bins. The subprocess contributions are grouped into seven categories according to the type of the incoming partons. The notation implies the sum over initial-state parton flavors as well as interchanged quarks and antiquarks.

all PF candidates in the event. Its magnitude is referred to as $E_{\mathrm{T}}^{\mathrm{miss}}$. Dijet events exhibit little missing transverse energy $E_{\mathrm{T}}^{\mathrm{miss}}$, which is required to be smaller than 30% of the total transverse energy.

3 Measurement of triple-differential dijet cross sections

The triple-differential cross section for dijet production is defined as

$$\frac{d^3\sigma}{dp_{\mathrm{T,avg}}dy^*dy_{\mathrm{b}}} = \frac{1}{\epsilon\mathcal{L}_{\mathrm{int}}^{\mathrm{eff}}}\frac{N}{\Delta p_{\mathrm{T,avg}}\Delta y^*\Delta y_{\mathrm{b}}},$$

where N denotes the number of dijet events, $\mathcal{L}_{\mathrm{int,eff}}$ the effective integrated luminosity and ϵ the product of trigger and event selection efficiencies which are greater than 99% in the measured phase space. Contributions from background processes like $t\bar{t}$ production are several orders of magnitude smaller and are neglected. The cross section is normalized by the widths of the bins, $\Delta p_{\mathrm{T,avg}}$, Δy^*, and Δy_{b}, respectively.

The cross sections are unfolded to stable particle level (lifetime $c\tau > 1$ cm) to correct for the detector resolution effects. The iterative D'Agostini algorithm [23], as implemented in the RooUnfold package [24], is employed. The response matrix, which maps the particle-level distribution to the measured distribution, is derived from simulation. An NLOJET++ prediction, obtained with the CT14 PDF [25] and corrected for nonperturbative and electroweak effects, represents the distribution at particle level and is smeared using the jet p_{T} resolution to yield the measured distribution. The jet energy resolution (JER) is derived with the CMS detector simulation based on the GEANT4 toolkit [26] and the PYTHIA 6 Monte Carlo (MC) event generator [27] and is corrected for residual differences between data and simulation. The p_{T} resolution is about 8% at 100 GeV and improves to 5% at 1 TeV. The iterative unfolding procedure is regularized by the number of iterations, which is set to four. Due to bin migrations during the unfolding procedure, small correlations of the statistical uncertainties between neighbouring bins are introduced. The statistical uncertainties are smaller than 1% in the majority of the phase space and increase up to 20% for highest $p_{\mathrm{T,avg}}$.

The dominant systematic uncertainties in the cross section arise from uncertainties in the jet energy scale corrections and are about 2.5% in the central region and increase to 12% in the forward regions. The uncertainty on the luminosity of 2.6% directly propagates into the cross section. The uncertainty in the jet energy resolution enters the measurement through the unfolding procedure and results in an additional uncertainty of 1% to 2% on the unfolded cross section. Non-Gaussian tails in the detector response have a small influence in the forward region and cause an additional uncertainty of up to 2% there. Residual effects of small inefficiencies from the jet identification and trigger selection are covered by an uncorrelated uncertainty of 1%. Figure 3 depicts all experimental uncertainties as well as the total uncertainty, which is calculated as the quadratic sum of all individual sources.

4 Theory predictions

The NLO predictions of the triple-differential dijet cross section are calculated using NLOJET++, which is used within the framework of FASTNLO [28, 29]. The renormalization and factorization scales μ_r and μ_f are both set to $\mu = \mu_0 = p_{\mathrm{T,max}} \cdot e^{0.3y^*}$, a scale choice first investigated in [30]. Compared to a prediction with $\mu = p_{\mathrm{T,avg}}$, the scale uncertainties are reduced for regions with large values of y_{b}. The predictions for cross sections obtained with different central

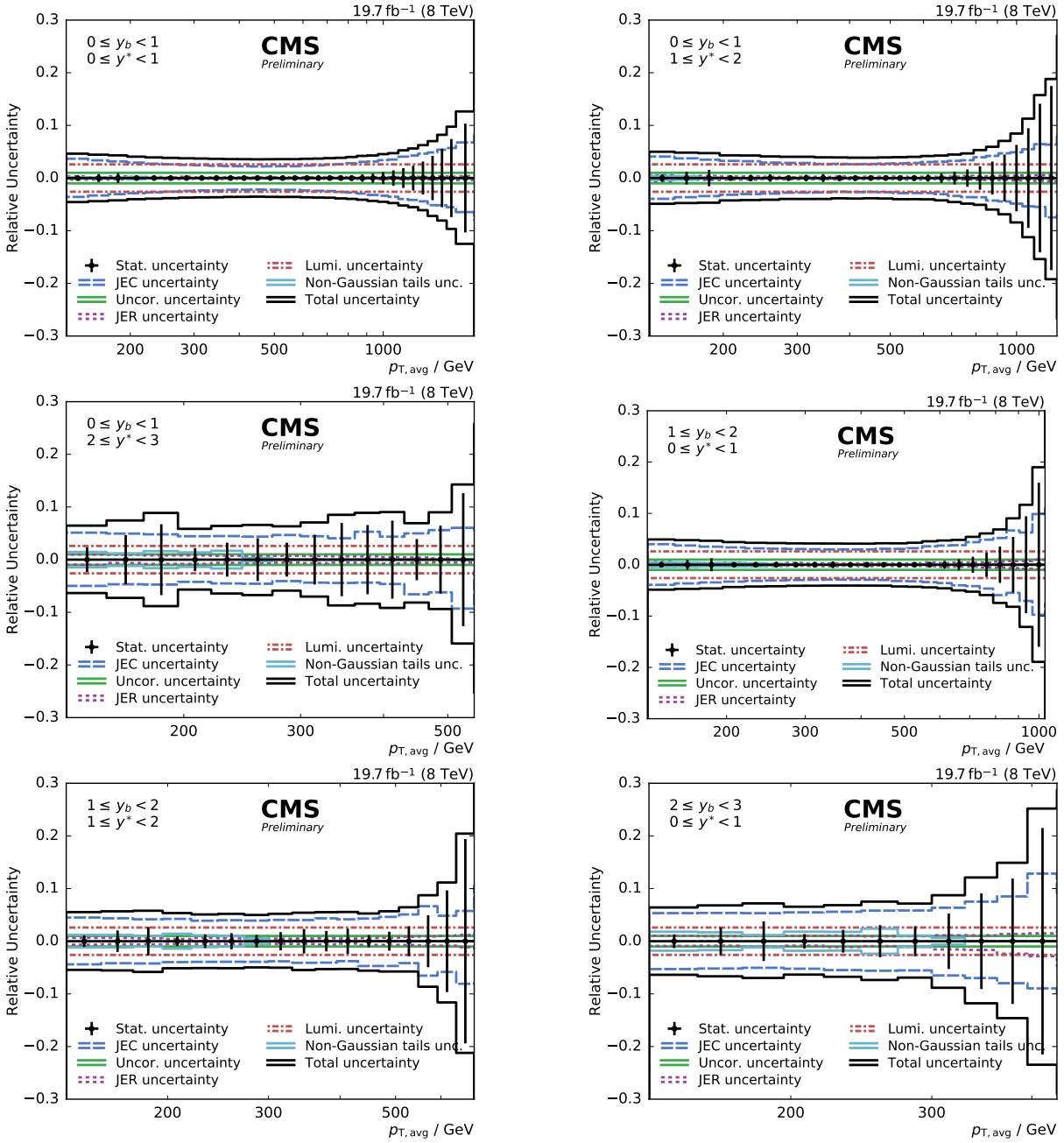

Figure 3: Overview of all experimental uncertainties affecting the cross section measurement. The error bars indicate the statistical uncertainty after unfolding. The different lines give the uncertainties resulting from jet energy corrections, jet energy resolution, luminosity, non-Gaussian tail, and residual effects. The total uncertainty is obtained by adding quadratically the individual sources of uncertainty.

scale choices are consistent within the scale uncertainties. The calculation is performed using the four PDF sets CT14, ABM11 [31], MMHT2014 [32] and NNPDF 3.0 [33] at next-to-leading evolution order and are accessed via the LHAPDF interface [34, 35] using the respective values of $\alpha_S(M_Z)$ and the supplied α_S evolution.

The fixed-order calculations are accompanied by NP corrections c_k^{NP} derived from the LO MC generators PYTHIA 8 [36] and HERWIG++ [37] with the tunes CUETP8M1 and UE-EE-5C [38] and the NLO MC generator POWHEG [39–42] in combination with PYTHIA 8 and the tunes CUETP8M1 and CUETP8S1 [38].

The correction factor c_k^{NP} is defined as the ratio between the nominal cross section with and without multi-parton interactions (MPI) and hadronization (HAD) effects

$$c_k^{\mathrm{NP}} = \frac{\sigma^{\mathrm{PS+HAD+MPI}}}{\sigma^{\mathrm{PS}}},$$

where the superscript indicates the applied steps in the simulation: the parton shower (PS), the MPI and the hadronization. The corresponding correction factor is applied in each bin to the parton-level NLO cross section. It differs from unity by about 10% for lowest $p_{\mathrm{T,avg}}$ and decreases to zero deviation above 1 TeV.

To account for differences of the correction factors obtained by using HERWIG++, PYTHIA 8, and POWHEG +PYTHIA 8, half of the envelope of all these predictions is taken as uncertainty and the mean of the envelope is used as central correction factor.

The contribution of electroweak effects [43], which dominantly arise from virtual exchanges of massive W and Z bosons, become relevant at high jet p_{T} and central rapidities. The corrections are smaller than 3% below 1 TeV and reach 8% for the highest $p_{\mathrm{T,avg}}$. Uncertainties on this small correction are assumed to be negligible.

The total theory uncertainty is obtained as the quadratic sum of NP, scale, and PDF uncertainties. The scale uncertainties are calculated by varying μ_r and μ_f using multiplicative factors in the following six combinations: $(\mu_r/\mu_0, \mu_f/\mu_0) = (1/2, 1/2)$, $(1/2, 1)$, $(1, 1/2)$, $(1, 2)$, $(2, 1)$ and $(2, 2)$. The uncertainty is determined as the maximal upwards and downwards variation with respect to the cross section obtained with the nominal scale setting [44, 45]. The PDF uncertainties are evaluated according to the NNPDF 3.0 PDF prescription. Figure 4 shows the relative size of the uncertainties for the studied phase space regions.

5 Results

The triple-differential dijet cross sections are presented in Fig. 5 as a function of $p_{\mathrm{T,avg}}$ for six phase space regions in y^* and y_{b}. The unfolded cross sections are compared to predictions as derived in the previous section. The data are compatible with theory over a wide range of the investigated phase space.

The ratio of data over theory is shown in Fig. 6 for predictions using various global PDF sets. The data are well described by the predictions using the CT14, MMHT 2014, and NNPDF 3.0 PDFs in most of the analysed phase space. In the boosted regions ($y_{\mathrm{b}} \geq 1$) differences between data and predictions are observed at high $p_{\mathrm{T,avg}}$, where the less known high-x region of the PDFs is probed. In this boosted dijet topology, the predictions exhibit large PDF uncertainties, as can be seen in Fig. 4. The significantly smaller uncertainties of the data in that region indicate the possibility to constrain the PDFs.

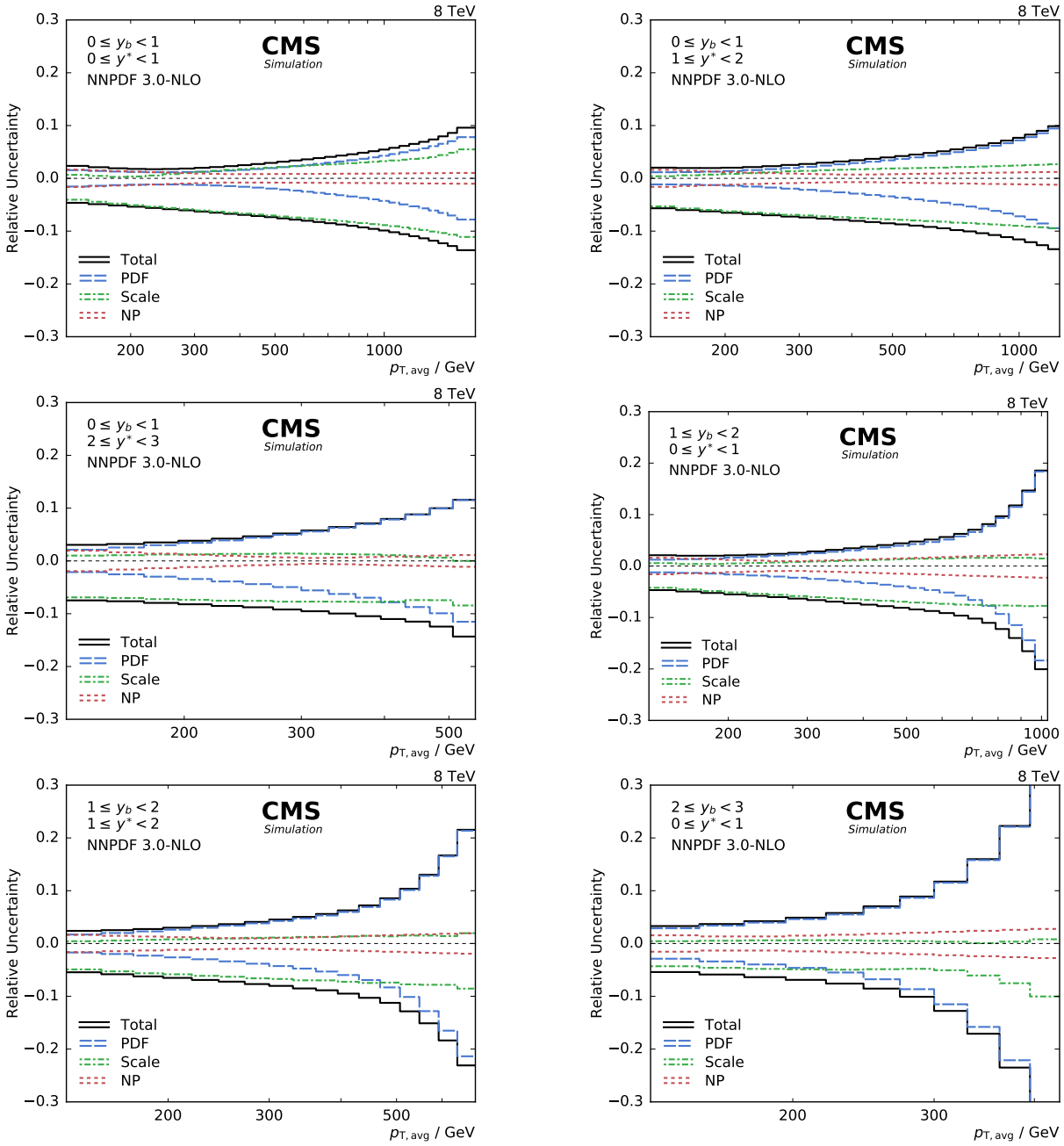

Figure 4: Overview of theory uncertainties. The scale uncertainty dominates in the low-$p_{T,avg}$ region. At high-$p_{T,avg}$ and especially in the boosted region, the PDFs become the dominant source of uncertainty.

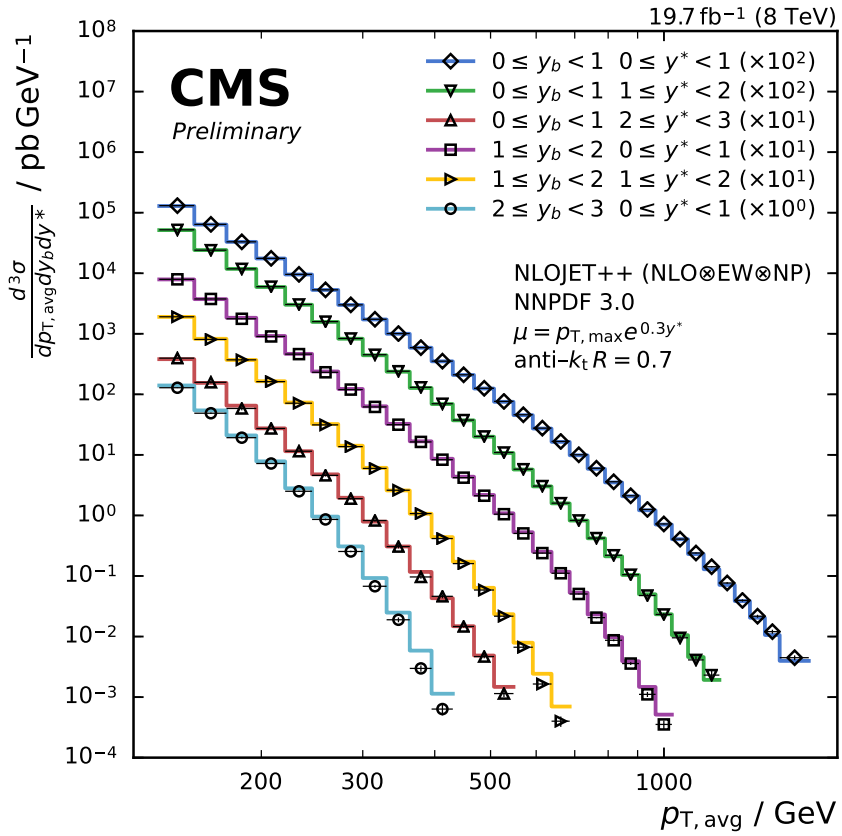

Figure 5: The triple-differential dijet cross section in six bins of y^* and y_b. The data are indicated by different markers for each bin and the theory obtained with NLOJET++ and NNPDF 3.0, complemented with EW and NP corrections, is depicted by solid lines. Apart from the boosted region, the data are well described by NLO theory calculations over many orders of magnitude.

Predictions using the ABM 11 PDFs systematically underestimate the data in the central region. This behavior has been observed previously [46] and can be traced back to a soft gluon PDF accompanied with a low value of $\alpha_S(M_Z)$ in the PDF.

Figure 7 presents in addition the ratios of the data to the predictions of the POWHEG +PYTHIA 8 and HERWIG 7 [47] NLO MC event generators. Significant differences between the predictions of both MC event generators are observed. However, the scale definitions as well as the used PDF sets are different. POWHEG and HERWIG 7 are using the CT10 and MMHT 2014 PDF sets, respectively. In general, HERWIG 7 better describes the data in the central region while POWHEG prevails in the boosted region.

6 PDF constraints

The constraints of the triple-differential dijet measurement on the proton PDFs are demonstrated by including the cross sections in a PDF fit together with inclusive DIS cross section measurements from the HERA experiments [48]. The fit is performed with XFITTER [49], an open source framework developed to fit the PDFs to experimental data. The PDF evolution is based on the DGLAP [50–52] evolution equations. To ensure consistency between the HERA DIS and the dijet cross section calculations, the fits are performed at NLO as the latter were only available at that order. The DIS cross sections are calculated by the QCDNUM software [53].

The QCD analysis is based on similar studies of inclusive jet data at 7 TeV [46] and 8 TeV [54] and all settings were set in accordance to the inclusive jet study at 8 TeV [54]. The parametrization of the PDFs is defined at the starting scale $Q_0^2 = 1.9\,\text{GeV}^2$ and the five independent PDFs $xu_v(x)$, $xd_v(x)$, $xg(x)$, $x\bar{U}(x)$, and $x\bar{D}(x)$ are parametrized as follows:

$$xg(x) = A_g x^{B_g}(1-x)^{C_g} - A'_g x^{B'_g}(1-x)^{C'_g} \tag{1}$$

$$xu_v(x) = A_{u_v} x^{B_{u_v}}(1-x)^{C_{u_v}}(1 + D_{u_v}x + E_{u_v}x^2) \tag{2}$$

$$xd_v(x) = A_{d_v} x^{B_{d_v}}(1-x)^{C_{d_v}}(1 + D_{d_v}x) \tag{3}$$

$$x\bar{U}(x) = A_{\bar{U}} x^{B_{\bar{U}}}(1-x)^{C_{\bar{U}}}(1 + D_{\bar{U}}x) \tag{4}$$

$$x\bar{D}(x) = A_{\bar{D}} x^{B_{\bar{D}}}(1-x)^{C_{\bar{D}}}\,. \tag{5}$$

Out of these, the normalization parameters A_g, A_{u_v}, and A_{d_v} are fixed using QCD sum rules. $B_{\bar{U}} = B_{\bar{D}}$ and $A_{\bar{U}} = A_{\bar{D}}(1 - f_s)$ are imposed to ensure the same normalization for the $\bar{u}$ and $\bar{d}$ PDF for the $x \to 0$ region. The strange quark PDF is determined as a fixed fraction $f_s = 0.31$ of $x\bar{D}(x)$. The generalized-mass variable-flavor-number-scheme as described in [55, 56] is used and the strong coupling constant is set to $\alpha_S(M_Z) = 0.1180$. The parameters in Equations 1–5 are selected by first performing fits where all D and E parameters are set to zero. Further parameters are then included into the fit one at a time. The improvement of χ^2 of the fit is monitored and the procedure is stopped when no further improvement is observed. This leads to a 16 parameter fit. Due to differences in the sensitivity to the different PDFs of dijet and inclusive jet data, the parametrisation of the present analysis differs from that in [54]. In particular, the relation $B_{d_v} = B_{u_v}$ at the starting scale could be released. This results in a d valence distribution well consistent with the results obtained in [54] and the QCD analysis of muon charge asymmetry in W-boson production at 8 TeV [57].

The PDF uncertainties are determined using the HERAPDF method, in which the uncertainties are subdivided into three independent sources, which are evaluated separately and added in

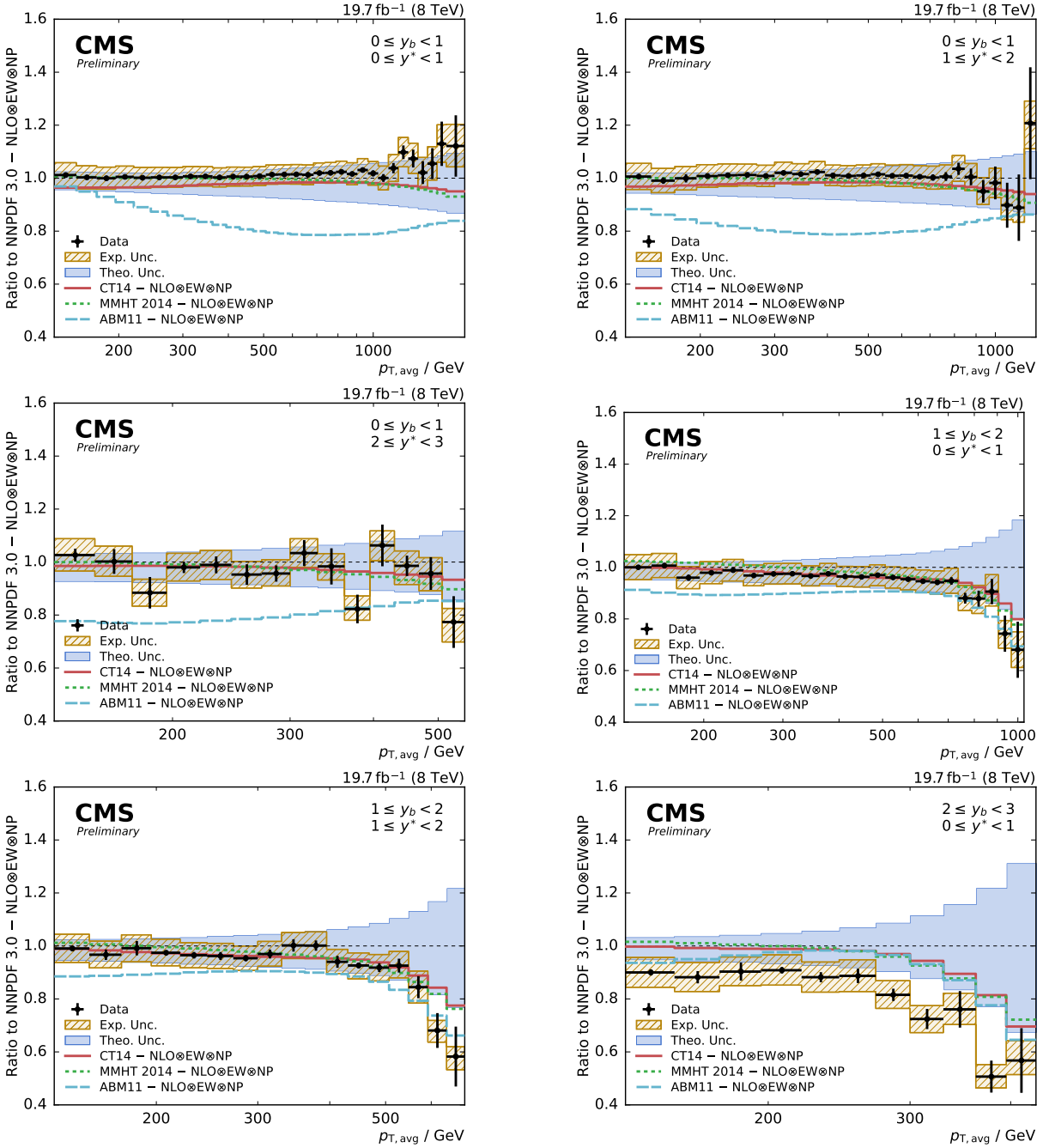

Figure 6: Ratio of the triple-differential dijet cross section to the NLOJET++ prediction using the NNPDF 3.0 set. The data points including statistical uncertainties are indicated by markers, the total experimental uncertainty is represented by the hatched band. The solid band shows the PDF, scale, and NP uncertainties quadratically added, the solid and dashed lines give the predictions calculated with different PDF sets.

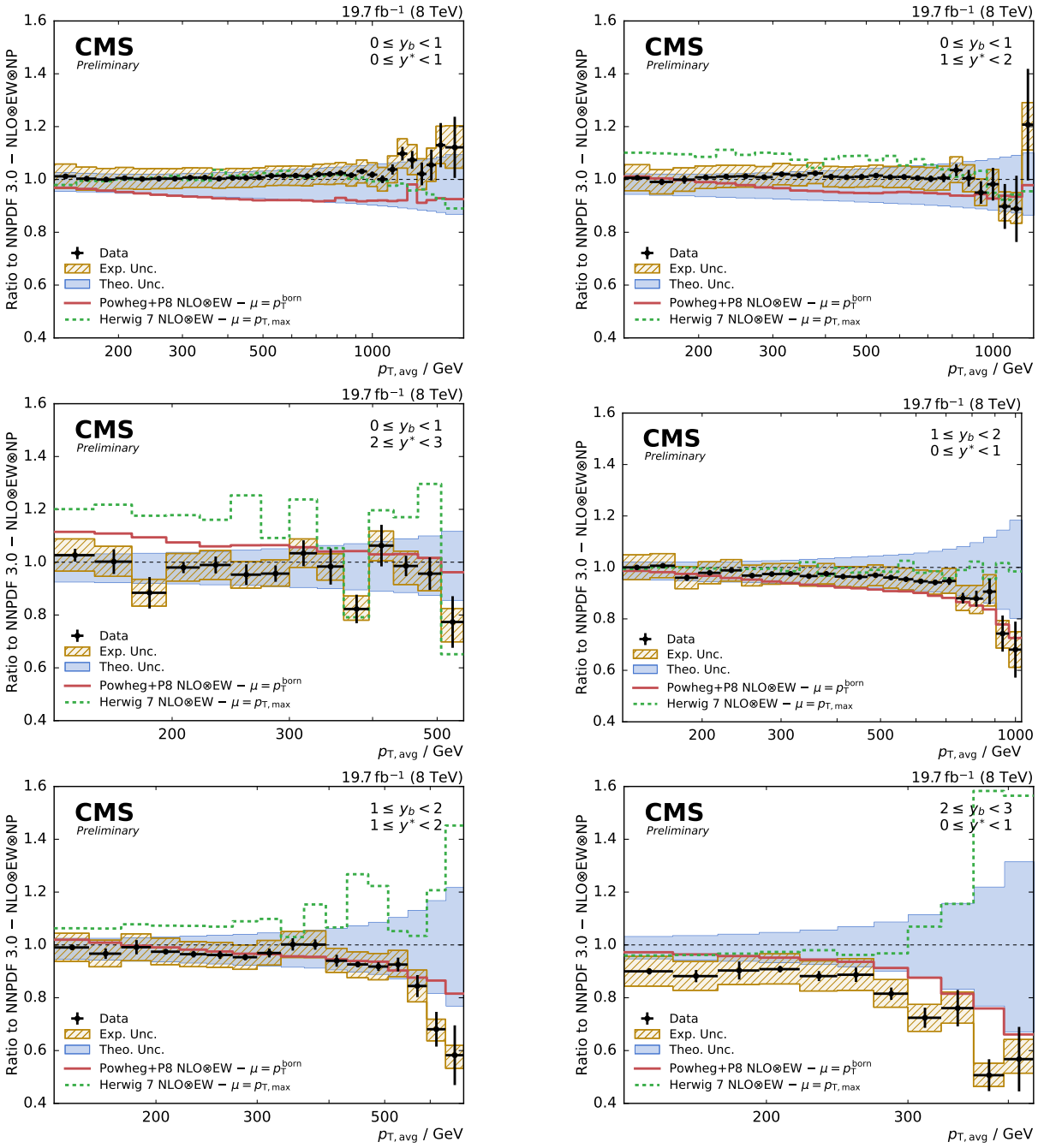

Figure 7: Ratio of the triple-differential dijet cross sections to the NLOJET++ prediction using the NNPDF 3.0 set. The data points including statistical uncertainties are indicated by markers, the total experimental uncertainty is represented by the hatched band. The solid band shows the PDF, scale, and NP uncertainties quadratically added. The predictions of the NLO MC event generators POWHEG +PYTHIA 8 and HERWIG 7 are depicted by solid and dashed lines, respectively.

quadrature to obtain the total PDF uncertainty.

Experimental uncertainties originate from statistical and systematic uncertainties of the data and are propagated to the PDFs using the Hessian eigenvector method [58] and a tolerance criterion of $\Delta\chi^2 = +1$. Alternatively, the Monte-Carlo method [59] is used to determine the PDF fit uncertainties and qualitatively similar results are obtained.

The uncertainties of several input parameters in the PDF fits are combined into one model uncertainty. For the evaluation of the model uncertainties, the following variations on the input parameters are considered:

The strangeness fraction $f_s = 0.31$ is varied between 0.23 and 0.39. The b-quark mass, set to 4.5 GeV, is varied between 4.25 GeV and 4.75 GeV. The c-quark mass, set by default to 1.47 GeV, is varied between 1.41 GeV and 1.53 GeV. The Q^2 cut imposed on the HERA DIS data $Q^2_{\text{min}} = 7.5\,\text{GeV}^2$, is varied to $Q^2_{\text{min}} = 5.0\,\text{GeV}^2$ and $Q^2_{\text{min}} = 10.0\,\text{GeV}^2$.

The parametrization uncertainty is estimated by including additional parameters in the fit, leading to a more flexible functional form of the PDFs. Each parameter is successively added in the PDF fit and the envelope of all changes to the central PDF fit result is taken as parametrization uncertainty. Furthermore, the variation of the starting scale Q^2_0 to 1.6 GeV^2 and 2.2 GeV^2 is treated as parametrization variation.

The quality of the fit with and without the dijet measurement is reported in Table 2. The partial χ^2 per data point for each data set as well as the χ^2 per number of degrees of fredom, n_{dof}, for all data sets demonstrate the compatibility of the CMS dijet measurement and the DIS data from the HERA experiments in a combined fit.

Table 2: The partial χ^2 for each data set in the HERA DIS (middle section) or the combined fit including the triple-differential dijet data (right section) are shown. The bottom two lines show the total χ^2 and χ^2/n_{dof}. The difference between the sum of all χ^2_{p} and the total χ^2 for the combined fit is attributed to the nuisance parameters.

		HERA data		**HERA & CMS data**	
data set	n_{data}	χ^2_{p}	$\chi^2_{\text{p}}/n_{\text{data}}$	χ^2_{p}	$\chi^2_{\text{p}}/n_{\text{data}}$
NC HERA-I+II e^+p $E_{\text{p}} = 920\,\text{GeV}$	332	382.44	1.15	406.45	1.22
NC HERA-I+II e^+p $E_{\text{p}} = 820\,\text{GeV}$	63	60.62	0.96	61.01	0.97
NC HERA-I+II e^+p $E_{\text{p}} = 575\,\text{GeV}$	234	196.40	0.84	197.56	0.84
NC HERA-I+II e^+p $E_{\text{p}} = 460\,\text{GeV}$	187	204.42	1.09	205.50	1.10
NC HERA-I+II e^-p	159	217.27	1.37	219.17	1.38
CC HERA-I+II e^+p	39	43.26	1.11	42.29	1.08
CC HERA-I+II e^-p	42	49.11	1.17	55.35	1.32
CMS Triple-Differential Dijets	122	—	—	111.13	0.91
data set(s)	n_{dof}	χ^2	χ^2/n_{dof}	χ^2	χ^2/n_{dof}
HERA data	1040	1211.00	1.16	—	—
HERA & CMS data	1162	—	—	1372.52	1.18

The obtained PDFs for the gluon, u valence, d valence, and sea quark are presented for a fit with and without the CMS dijet data in Fig. 8 for $Q^2 = 10^4\,\text{GeV}^2$. The uncertainty of the gluon PDF is reduced over a large range in x. The impact is largest in the high-x region and comes along with a noticeable change in shape of the gluon PDF when evolved to low scales. Compared to

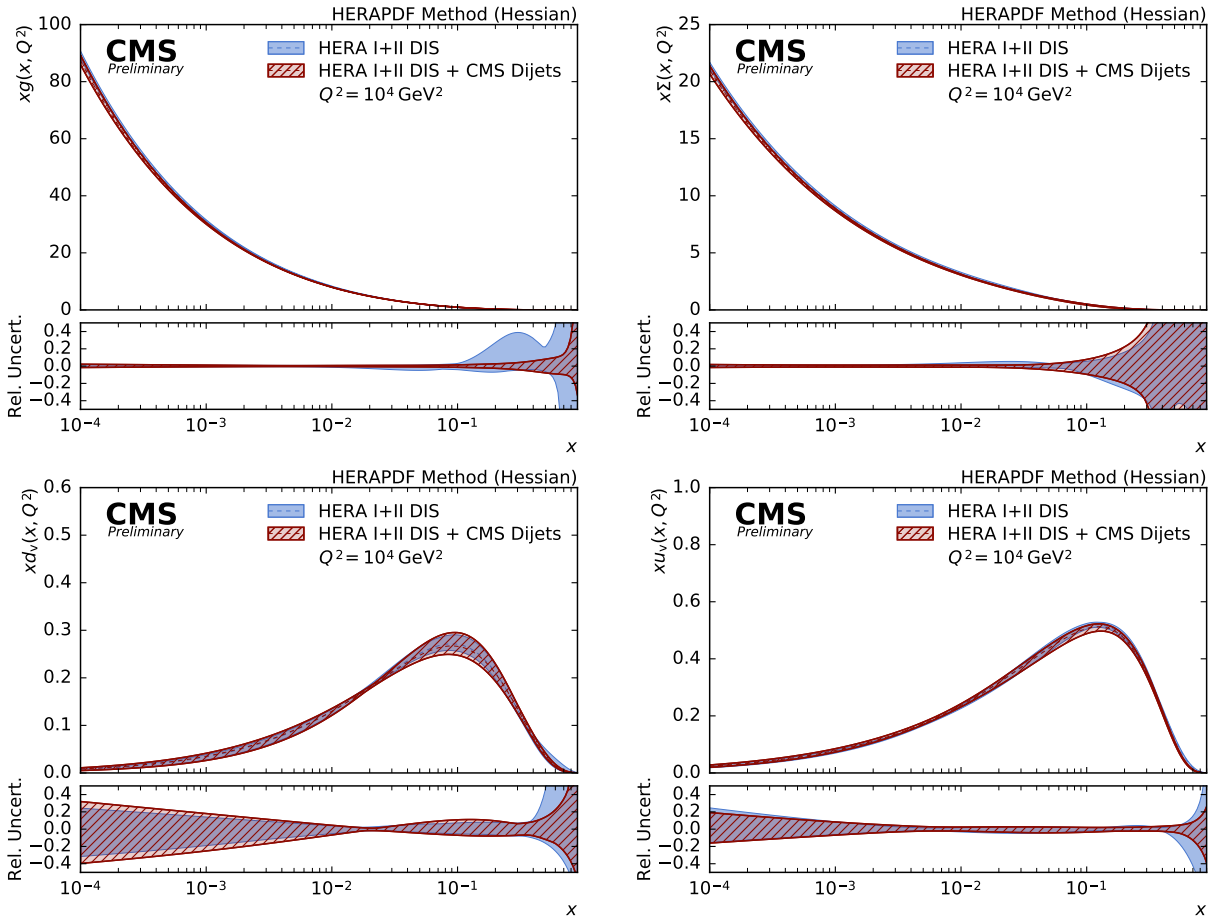

Figure 8: The gluon (top left), sea quark (top right), d valence quark (bottom left) and u valence quark (bottom right) PDFs as a function of x as derived from HERA inclusive DIS data alone (hatched band) and in combination with CMS dijet data (solid band). The PDFs are shown at the scale $Q^2 = 10^4\,\mathrm{GeV}^2$ with their total uncertainties.

the fit with HERA DIS data alone, the gluon PDF decreases at medium x and increases at high x. Similar effects were observed before, e.g. in Ref. [46]. The valence quark PDFs and the sea quark PDFs exhibit reduced uncertainties in the high-x region as well. For x values beyond $\approx$ 0.7 or below 10^{-3} the extracted PDFs are not directly constrained by data and should be considered as extrapolations that rely on PDF parameterization assumptions alone. The PDFs are compared to those obtained with inclusive jet data at $\sqrt{s} = 8\,\mathrm{TeV}$ in Fig. 9. The shapes of the PDFs and the uncertainties are similar. Somewhat larger uncertainties in the valence quark distributions observed in the fit using the dijet data with respect to those obtained from inclusive jet cross sections can be explained by stronger sensitivity of the dijet data to the light quark distributions, resulting in an increased flexibility of the PDF parametrisation, however at the cost of an increased uncertainty.

The measurement of triple-differential dijet cross sections not only provides constraints on the PDFs, but also on the strong coupling constant. Therefore, the PDF fit is repeated with an additional free parameter: the strong coupling constant $\alpha_S(M_Z)$. The uncertainties are determined in the same way as in the PDF determination. The obtained value for the strong coupling constant reads

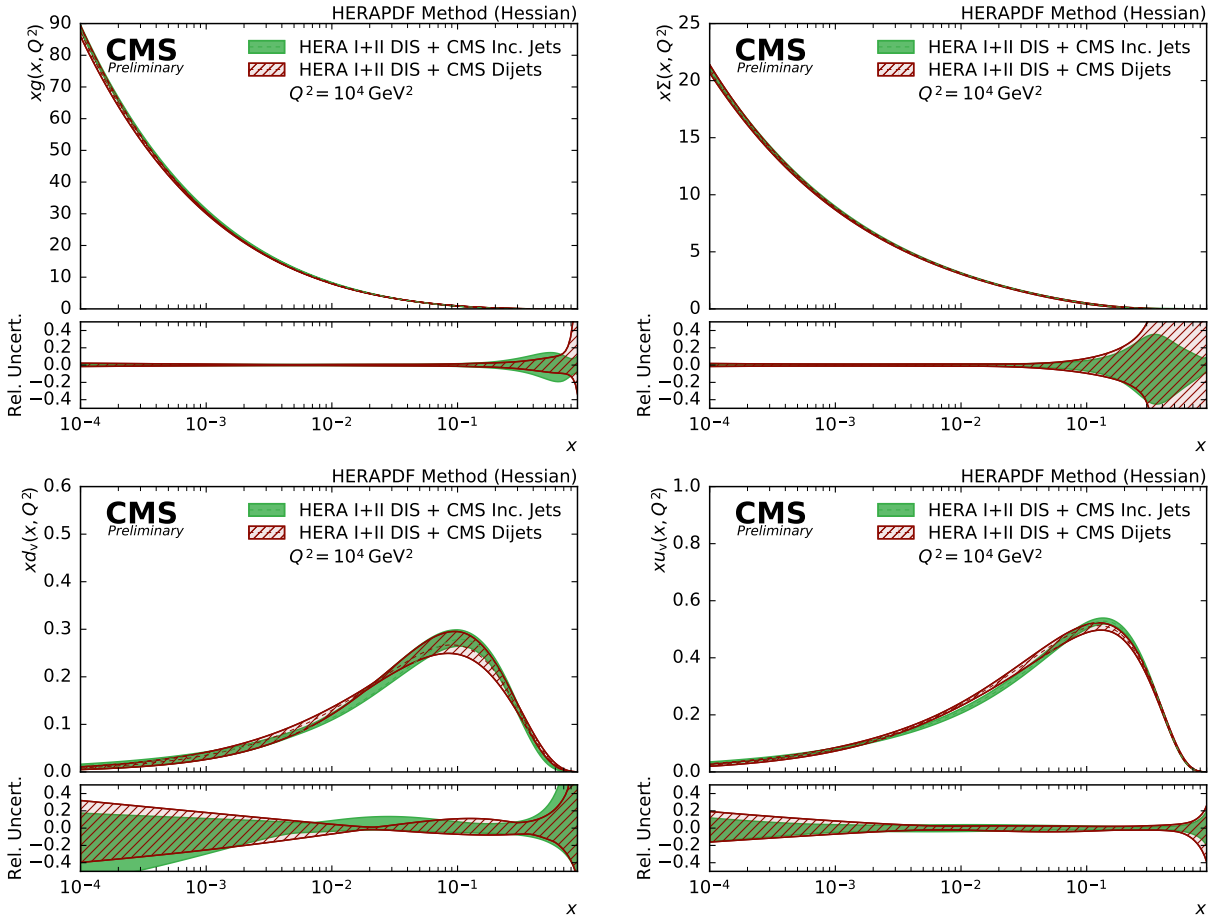

Figure 9: The gluon (top left), sea quark (top right), d valence quark (bottom left) and u valence quark (bottom right) PDFs as a function of x as derived from a fit of HERA inclusive DIS data in combination with CMS inclusive jet data (solid band) and CMS dijet data (hatched band) at 8 TeV. The PDFs are shown at the scale $Q^2 = 10^4\,\mathrm{GeV}^2$ with their total uncertainties.

$$\alpha_S(M_Z) = 0.1199 \pm 0.0015(\text{exp})^{+0.0002}_{-0.0002}(\text{mod})^{+0.0002}_{-0.0004}(\text{par}),$$

where the quoted experimental uncertainty accounts for all sources of uncertainties of the HERA and CMS data sets as well as the NP uncertainties. The consideration of scale uncertainties in a PDF fit is an open issue in the PDF community as they cannot be treated as Gaussian and therefore are not taken into account in any PDF fit. Two different methods to evaluate the scale uncertainty on $\alpha_S(M_Z)$ were studied: First, the renormalization and factorization scales were varied in the calculation of the dijet data. The fit was repeated for each variation. The uncertainty is evaluated as detailed in Sec. 4 and yields $\Delta\alpha_S(M_Z) = ^{+0.0026}_{-0.0016}$ (scale).

The second procedure is analogous to the method which was applied in previous determinations of $\alpha_S(M_Z)$, e.g. in Ref. [46, 60]. The PDFs are derived for a series of fixed values of $\alpha_S(M_Z)$. Using this series, the best fit $\alpha_S(M_Z)$ value of the dijet data is determined for each scale variation. Here, the evaluated uncertainty is $\Delta\alpha_S(M_Z) = ^{+0.0031}_{-0.0019}$ (scale). Since this uncertainty is the most consistent to be compared with previous determinations of $\alpha_S(M_Z)$, it is quoted as the main result.

The determined value of $\alpha_S(M_Z)$ is in agreement with the world average of $\alpha_S(M_Z) = 0.1181 \pm 0.0013$ [61] and with the result of the similar analysis using inclusive jet data [46]. In all cases, the dominant source of uncertainty is of theoretical origin.

7 Summary

A measurement of triple-differential dijet cross sections has been presented. The data were found to be well described by NLO predictions corrected for NP and EW effects except for a boosted event topology, which suffers from large PDF uncertainties. The precise data constrain the PDFs, especially in the boosted regime, where the highest momentum fractions x of the PDFs are probed. The impact of the data on the PDFs was demonstrated by performing a simultaneous fit to DIS cross sections obtained from the HERA experiments and the dijet cross sections measured in this paper. If the dijet data are considered, a slightly harder gluon PDF is obtained and the overall uncertainties of the PDFs, especially those of the gluon PDF, are significantly reduced.

The strong coupling constant $\alpha_S(M_Z)$ has been determined together with the PDFs in a simultaneous fit. The value obtained reads

$$\alpha_S(M_Z) = 0.1199 \pm 0.0015\,(\text{exp}) \pm 0.0002\,(\text{mod})\,^{+0.0002}_{-0.0004}\,(\text{par})\,^{+0.0031}_{-0.0019}\,(\text{scale})$$

and is in agreement with the world average value of $\alpha_S(M_Z) = 0.1181 \pm 0.0013$ determined by the PDG in the spring 2015 update of Ref. [61]. The dominant uncertainty is of theoretical origin that might be improved significantly in the future with the help of pQCD predictions at next-to-next-to-leading order [62].

References

[1] UA2 Collaboration, "Observation of Very Large Transverse Momentum Jets at the CERN $\bar{p}p$ Collider", *Phys. Lett. B* **118** (1982) 203, doi:10.1016/0370-2693(82)90629-3.

[2] AFS Collaboration, "Dijet Production Cross-Section and Fragmentation of Jets Produced in pp Collisions at $\sqrt{s} = 63\,\text{GeV}$", *Z. Phys. C* **30** (1986) 27, doi:10.1007/BF01560675.

[3] CDF Collaboration, "A measurement of the differential dijet mass cross section in $p\bar{p}$ collisions at $\sqrt{s} = 1.8$ TeV", *Phys. Rev. D* **61** (2000) 091101, doi:10.1103/PhysRevD.61.091101, arXiv:hep-ex/9912022.

[4] CDF Collaboration, "Measurement of the dijet mass distribution in $p\bar{p}$ collisions at $\sqrt{s} = 1.8$ TeV", *Phys. Rev. D* **48** (1993) 998, doi:10.1103/PhysRevD.48.998.

[5] CDF Collaboration, "Two-jet invariant-mass distribution at $\sqrt{s} = 1.8$ TeV", *Phys. Rev. D* **41** (1990) 1722, doi:10.1103/PhysRevD.41.1722.

[6] D0 Collaboration, "The dijet mass spectrum and a search for quark compositeness in $\bar{p}p$ collisions at $\sqrt{s} = 1.8$ TeV", *Phys. Rev. Lett.* **82** (1999) 2457, doi:10.1103/PhysRevLett.82.2457, arXiv:hep-ex/9807014.

[7] ATLAS Collaboration, "Measurement of inclusive jet and dijet cross sections in proton-proton collisions at 7 TeV centre-of-mass energy with the ATLAS detector", *Eur. Phys. J. C* **71** (2011) 1512, doi:10.1140/epjc/s10052-010-1512-2, arXiv:1009.5908.

[8] CMS Collaboration, "Measurement of the differential dijet production cross section in proton-proton collisions at $\sqrt{s} = 7$ TeV", *Phys. Lett. B* **700** (2011) 187, doi:10.1016/j.physletb.2011.05.027, arXiv:1104.1693.

[9] ATLAS Collaboration, "Measurement of inclusive jet and dijet production in pp collisions at $\sqrt{s} = 7$ TeV using the ATLAS detector", *Phys. Rev. D* **86** (2012) 014022, doi:10.1103/PhysRevD.86.014022, arXiv:1112.6297.

[10] ATLAS Collaboration, "Measurement of dijet cross sections in pp collisions at 7 TeV centre-of-mass energy using the ATLAS detector", *JHEP* **05** (2014) 059, doi:10.1007/JHEP05(2014)059, arXiv:1312.3524.

[11] CMS Collaboration, "Measurements of differential jet cross sections in proton-proton collisions at $\sqrt{s} = 7$ TeV with the CMS detector", *Phys. Rev. D* **87** (2013) 112002, doi:10.1103/PhysRevD.87.112002, arXiv:1212.6660.

[12] CDF Collaboration, "Two-Jet Differential Cross-Section in $\bar{p}p$ Collisions at $\sqrt{s} = 1.8$ TeV", *Phys. Rev. Lett.* **64** (1990) 157, doi:10.1103/PhysRevLett.64.157.

[13] CDF Collaboration, "Measurement of the two-jet differential cross section in $p\bar{p}$ collisions at $\sqrt{s} = 1800$ GeV", *Phys. Rev. D* **64** (2001) 012001, doi:10.1103/PhysRevD.65.039902, 10.1103/PhysRevD.64.012001, arXiv:hep-ex/0012013.

[14] Z. Nagy, "Three jet cross-sections in hadron hadron collisions at next-to-leading order", *Phys. Rev. Lett.* **88** (2002) 122003, doi:10.1103/PhysRevLett.88.122003, arXiv:hep-ph/0110315.

[15] Z. Nagy, "Next-to-leading order calculation of three-jet observables in hadron hadron collisions", *Phys. Rev. D* **68** (2003) 094002, doi:10.1103/PhysRevD.68.094002, arXiv:hep-ph/0307268.

[16] CMS Trigger and Data Acquisition Group Collaboration, "The CMS high level trigger", *Eur. Phys. J. C* **46** (2006) 605, doi:10.1140/epjc/s2006-02495-8, arXiv:hep-ex/0512077.

[17] CMS Collaboration, "Particle-Flow Event Reconstruction in CMS and Performance for Jets, Taus, and MET", Technical Report CMS-PAS-PFT-09-001, CERN, 2009.

[18] CMS Collaboration, "Particle-flow commissioning with muons and electrons from J/Psi and W events at 7 TeV", Technical Report CMS-PAS-PFT-10-003, CERN, 2010.

[19] CMS Collaboration, "Pileup Removal Algorithms",.

[20] M. Cacciari, G. P. Salam, and G. Soyez, "The anti-k_t jet clustering algorithm", *JHEP* **04** (2008) 063, doi:10.1088/1126-6708/2008/04/063, arXiv:0802.1189.

[21] M. Cacciari, G. P. Salam, and G. Soyez, "FastJet User Manual", *Eur. Phys. J. C* **72** (2012) 1896, doi:10.1140/epjc/s10052-012-1896-2, arXiv:1111.6097.

[22] CMS Collaboration, "Determination of Jet Energy Calibration and Transverse Momentum Resolution in CMS", *JINST* **6** (2011) P11002, doi:10.1088/1748-0221/6/11/P11002, arXiv:1107.4277.

[23] G. D'Agostini, "A Multidimensional unfolding method based on Bayes' theorem", *Nucl. Instrum. Meth. A* **362** (1995) 487, doi:10.1016/0168-9002(95)00274-X.

[24] T. Adye, "Unfolding algorithms and tests using RooUnfold", in *Proceedings, PHYSTAT 2011 Workshop on Statistical Issues Related to Discovery Claims in Search Experiments and Unfolding*, p. 313. Geneva, Switzerland, January 17-20, 2011. arXiv:1105.1160. doi:10.5170/CERN-2011-006.

[25] S. Dulat et al., "New parton distribution functions from a global analysis of quantum chromodynamics", *Phys. Rev. D* **93** (2016), no. 3, 033006, doi:10.1103/PhysRevD.93.033006, arXiv:1506.07443.

[26] S. Agostinelli et al., "GEANT4: A Simulation toolkit", *Nuclear Instruments & Methods in Physics Research A* **506** (2003) 250, doi:10.1016/S0168-9002(03)01368-8.

[27] T. Sjstrand, S. Mrenna, and P. Z. Skands, "PYTHIA 6.4 Physics and Manual", *JHEP* **05** (2006) 026, doi:10.1088/1126-6708/2006/05/026, arXiv:hep-ph/0603175.

[28] T. Kluge, K. Rabbertz, and M. Wobisch, "fastNLO: Fast pQCD calculations for PDF fits", in *14th International Workshop on Deep Inelastic Scattering (DIS 2006)*, p. 483. Tsukuba, Japan, April 20-24, 2006. arXiv:hep-ph/0609285. doi:10.1142/9789812706706_0110.

[29] D. Britzger, K. Rabbertz, F. Stober, and M. Wobisch, "New features in version 2 of the fastNLO project", in *Proceedings, XX. International Workshop on Deep-Inelastic Scattering and Related Subjects (DIS 2012)*, p. 217. Bonn, Germany, March 26-30, 2012. arXiv:1208.3641. doi:10.3204/DESY-PROC-2012-02/165.

[30] S. D. Ellis, Z. Kunszt, and D. E. Soper, "Two-Jet Production in Hadron Collisions at Order α_s^3 in QCD", *Phys. Rev. Lett.* **69** (1992) 1496, doi:10.1103/PhysRevLett.69.1496.

[31] S. Alekhin, J. Blmlein, and S. Moch, "Parton Distribution Functions and Benchmark Cross Sections at NNLO", *Phys. Rev. D* **86** (2012) 054009, doi:10.1103/PhysRevD.86.054009, arXiv:1202.2281.

[32] L. A. Harland-Lang, A. D. Martin, P. Motylinski, and R. S. Thorne, "Parton distributions in the LHC era: MMHT 2014 PDFs", *Eur. Phys. J. C* **75** (2015), no. 5, 204, doi:10.1140/epjc/s10052-015-3397-6, arXiv:1412.3989.

[33] NNPDF Collaboration, "Parton distributions for the LHC Run II", *JHEP* **04** (2015) 040, doi:10.1007/JHEP04(2015)040, arXiv:1410.8849.

[34] M. R. Whalley, D. Bourilkov, and R. C. Group, "The Les Houches Accord PDFs (LHAPDF) and LHAGLUE", in *Proceedings, HERA and the LHC: A Workshop on the implications of HERA for LHC physics: Vol. B*. Geneva, Switzerland and Hamburg, Germany, March 26-27, October 11-13, March 21-24, 2004-2005. arXiv:hep-ph/0508110.

[35] A. Buckley et al., "LHAPDF6: parton density access in the LHC precision era", *Eur. Phys. J.* **C75** (2015) 132, doi:10.1140/epjc/s10052-015-3318-8, arXiv:1412.7420.

[36] T. Sjstrand, S. Mrenna, and P. Z. Skands, "A Brief Introduction to PYTHIA 8.1", *Comput. Phys. Commun.* **178** (2008) 852, doi:10.1016/j.cpc.2008.01.036, arXiv:0710.3820.

[37] M. Bhr et al., "Herwig++ Physics and Manual", *Eur. Phys. J. C* **58** (2008) 639, doi:10.1140/epjc/s10052-008-0798-9, arXiv:0803.0883.

[38] CMS Collaboration, "Event generator tunes obtained from underlying event and multiparton scattering measurements", *Eur. Phys. J. C* **76** (2015), no. 3, 155, doi:10.1140/epjc/s10052-016-3988-x, arXiv:1512.00815.

[39] P. Nason, "A New method for combining NLO QCD with shower Monte Carlo algorithms", *JHEP* **11** (2004) 040, doi:10.1088/1126-6708/2004/11/040, arXiv:hep-ph/0409146.

[40] S. Frixione, P. Nason, and C. Oleari, "Matching NLO QCD computations with Parton Shower simulations: the POWHEG method", *JHEP* **11** (2007) 070, doi:10.1088/1126-6708/2007/11/070, arXiv:0709.2092.

[41] S. Alioli, P. Nason, C. Oleari, and E. Re, "A general framework for implementing NLO calculations in shower Monte Carlo programs: the POWHEG BOX", *JHEP* **06** (2010) 043, doi:10.1007/JHEP06(2010)043, arXiv:1002.2581.

[42] S. Alioli et al., "Jet pair production in POWHEG", *JHEP* **04** (2011) 081, doi:10.1007/JHEP04(2011)081, arXiv:1012.3380.

[43] S. Dittmaier, A. Huss, and C. Speckner, "Weak radiative corrections to dijet production at the LHC", *PoS* **DIS2013** (2013) 283, arXiv:1306.6298.

[44] M. Cacciari et al., "The t anti-t cross-section at 1.8 TeV and 1.96 TeV: A Study of the systematics due to parton densities and scale dependence", *JHEP* **04** (2004) 068, doi:10.1088/1126-6708/2004/04/068, arXiv:hep-ph/0303085.

[45] A. Banfi, G. P. Salam, and G. Zanderighi, "Phenomenology of event shapes at hadron colliders", *JHEP* **06** (2010) 038, doi:10.1007/JHEP06(2010)038, arXiv:1001.4082.

[46] CMS Collaboration, "Constraints on parton distribution functions and extraction of the strong coupling constant from the inclusive jet cross section in pp collisions at $\sqrt{s} = 7$ TeV", *Eur. Phys. J. C* **75** (2015) 288, doi:10.1140/epjc/s10052-015-3499-1, arXiv:1410.6765.

[47] J. Bellm et al., "Herwig 7.0 / Herwig++ 3.0 Release Note", arXiv:1512.01178.

[48] H1, ZEUS Collaboration, "Combination of measurements of inclusive deep inelastic $e^{\pm}p$ scattering cross sections and QCD analysis of HERA data", *Eur. Phys. J. C* **75** (2015), no. 12, 580, doi:10.1140/epjc/s10052-015-3710-4, arXiv:1506.06042.

[49] S. Alekhin et al., "HERAFitter", *Eur. Phys. J. C* **75** (2015), no. 7, 304, doi:10.1140/epjc/s10052-015-3480-z, arXiv:1410.4412.

[50] V. N. Gribov and L. N. Lipatov, "Deep inelastic ep scattering in perturbation theory", *Sov. J. Nucl. Phys.* **15** (1972) 438.

[51] G. Altarelli and G. Parisi, "Asymptotic Freedom in Parton Language", *Nucl. Phys. B* **126** (1977) 298, doi:10.1016/0550-3213(77)90384-4.

[52] Y. L. Dokshitzer, "Calculation of the Structure Functions for Deep Inelastic Scattering and e+ e- Annihilation by Perturbation Theory in Quantum Chromodynamics.", *Sov. Phys. JETP* **46** (1977) 641.

[53] M. Botje, "QCDNUM: Fast QCD Evolution and Convolution", *Comput. Phys. Commun.* **182** (2011) 490, doi:10.1016/j.cpc.2010.10.020, arXiv:1005.1481.

[54] CMS Collaboration, "Measurement and QCD analysis of double-differential inclusive jet cross-sections in pp collisions at $\sqrt{s} = 8$ TeV and ratios to 2.76 and 7 TeV", arXiv:1609.05331.

[55] R. S. Thorne and R. G. Roberts, "An Ordered analysis of heavy flavor production in deep inelastic scattering", *Phys. Rev. D* **57** (1998) 6871, doi:10.1103/PhysRevD.57.6871, arXiv:hep-ph/9709442.

[56] R. S. Thorne, "Variable-flavor number scheme for next-to-next-to-leading order", *Phys. Rev. D* **73** (2006) 054019, doi:10.1103/PhysRevD.73.054019, arXiv:hep-ph/0601245.

[57] CMS Collaboration, "Measurement of the differential cross section and charge asymmetry for inclusive pp $\to W^{\pm} + X$ production at $\sqrt{s} = 8$ TeV", *Eur. Phys. J.* **C76** (2016), no. 8, 469, doi:10.1140/epjc/s10052-016-4293-4, arXiv:1603.01803.

[58] J. Pumplin et al., "Uncertainties of predictions from parton distribution functions. 2. The Hessian method", *Phys. Rev. D* **65** (2001) 014013, doi:10.1103/PhysRevD.65.014013, arXiv:hep-ph/0101032.

[59] W. T. Giele and S. Keller, "Implications of hadron collider observables on parton distribution function uncertainties", *Phys. Rev. D* **58** (1998) 094023, doi:10.1103/PhysRevD.58.094023, arXiv:hep-ph/9803393.

[60] CMS Collaboration, "Measurement of the inclusive 3-jet production differential cross section in proton-proton collisions at 7 TeV and determination of the strong coupling constant in the TeV range", *Eur. Phys. J. C* **75** (2015) 186, doi:10.1140/epjc/s10052-015-3376-y, arXiv:1412.1633.

[61] Particle Data Group Collaboration, "Review of Particle Physics", *Chin. Phys. C* **38** (2014) 090001, doi:10.1088/1674-1137/38/9/090001.

[62] J. Currie, E. W. N. Glover, and J. Pires, "NNLO QCD predictions for single jet inclusive production at the LHC", arXiv:1611.01460.